Production of ω and ϕ mesons in near-threshold πN reactions: Baryon resonances and the Okubo-Zweig-Iizuka rule

A. I. Titov,[1,2] B. Kämpfer,[1] and B. L. Reznik[3]
[1]*Forschungszentrum Rossendorf, PF 510119, D-01314 Dresden, Germany*
[2]*Bogolyubov Laboratory of Theoretical Physics, JINR, Dubna RU-141980, Russia*
[3]*Far-Eastern State University, Sukhanova 9, Vladivostok RU-690090, Russia*
(Received 25 July 2001; published 28 May 2002)

Results of a combined analysis are presented for the production of ω and ϕ mesons in πN reactions in the near-threshold region using a conventional ''nonstrange'' dynamics based on processes that are allowed by the nonideal ω-ϕ mixing. We show that the interferences of the t channel (meson exchange) and s, u channels (nucleon and nucleon-resonances) differ significantly for the ω and ϕ production amplitudes. This leads to a decrease of the relative yields, in comparison with the expectations based on a one-component amplitude with standard ω-ϕ mixing. We find a strong and nontrivial difference between observables in ω and ϕ production reactions caused by the different roles of the nucleon and nucleon-resonance amplitudes. A series of predictions for the experimental study of this effect is presented.

DOI: 10.1103/PhysRevC.65.065202 PACS number(s): 13.75.−n, 14.20.−c, 21.45.+v

I. INTRODUCTION

The present interest in a combined study of the ω and ϕ meson production in different elementary reactions is mainly related to the investigation of the hidden strangeness degrees of freedom in the nucleon. Since the ϕ meson is thought to consist mainly of strange quarks, its production should be suppressed according to the Okubo-Zweig-Iizuka (OZI) rule [1] if the entrance channel does not possess a considerable admixture of strangeness. The standard OZI rule violation is described by the deviation from the ideal ω-ϕ mixing by the angle $\Delta\theta_V \simeq 3.7°$ [2], which is a measure of the small contribution of light $u,\bar{u}$ and $d,\bar{d}$ quarks in the ϕ meson, or strange $s,\bar{s}$ quarks in the ω meson. Thus, the ratio of ω to ϕ production cross sections is expected to be $R^2_{\omega/\phi} \simeq \cot^2\Delta\theta_V \simeq 2.4\times 10^2$.

Indeed, the recent experiments on proton annihilation at rest (cf. [3] for references and a compilation of data) point to a large apparent violation of the OZI rule, which is interpreted [3,4] as a hint to an intrinsic $s\bar{s}$ component in the proton. However, the data can be explained as well by modified meson-exchange models [5] without introducing any strangeness component in the nucleon or OZI rule violation mechanisms.

On the other hand, the analysis of the πN sigma term [6] suggests that the proton might contain a strange quark admixture as large as 20%. Thus this issue remains controversial. Therefore it is tempting to look for other observables [3,7,8] that are sensitive to the strangeness content of the nucleon. Most of them are related to a possible strong interference of delicate $s\bar{s}$ knockout (or shake-off) amplitudes and the ''nonstrange'' amplitude, which is caused by OZI rule allowed processes, or by processes wherein the standard OZI rule violation comes from the ϕ-ω mixing.

A detailed analysis of the current status of the OZI rule in πN and NN reactions has been presented recently in [9]. It is shown in [9] that existing data for the ω and ϕ meson production in πN reactions give for the ratio of averaged amplitudes the value of $R_{\omega/\phi} = 8.7 \pm 1.8$, which is much smaller than the standard OZI rule violation value of $R^{OZI}_{\omega/\phi} = 15.43$ and may be interpreted as a hint to nonzero strangeness components in the nucleon.

Obviously, reliable information on a manifestation of hidden strangeness in the combined study of ϕ and ω production processes can be obtained only when the conventional, i.e., nonexotic, amplitudes have been understood quantitatively. The reaction $\pi N \to VN$ with $V = \omega,\ \phi$ has the evident advantage of being a simple hadronic reaction representing a subprocess, e.g., in $NN \to VNN$ reactions. The study of the former reactions is one of the objectives of the present work. The dominant conventional processes are depicted in Fig. 1, where (a) is the t channel meson-exchange process, while (b) depicts the s, u nucleon and nucleon-resonance channels. When taking separately each of these amplitudes, the ratio of ω to ϕ production amplitudes is proportional to $\cot\Delta\theta_V = 15.43$, and the question of how their coherent sum can result in a deviation from this value arises.

Note that most of the previous considerations of the possible violation of the OZI rule in hadronic reactions are based on one-component amplitudes in the spirit of [10,11]. But if one assumes that the process is a coherent sum of at least two amplitudes, say, for example, a meson-exchange and a nucleon term, then the result may be different from the

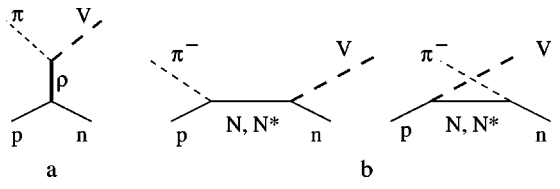

FIG. 1. Diagrammatic representation of the $\pi^- p \to Vn$ reaction mechanisms with $V = \omega,\ \phi$. (a) Meson-exchange diagram with vector-meson emission from the $V\rho\pi$ vertex, (b) nucleon and nucleon-resonance vector-meson production in the VNN and VNN^* vertices.

expectation resting on a one-component amplitude. Indeed, let us suppose for a moment that, because of some hadronic dynamics, the nucleon term for the ϕ production is suppressed relative to the meson-exchange term. This suppression might be caused by the baryon propagator, which is different for ϕ and ω production at the same energy excess because of the different thresholds. Then the ratio of ω to ϕ amplitudes becomes

$$R_{\omega/\phi}=\cot\Delta\theta_V\frac{|1+R^{\omega}_{N/M}|}{|1+R^{\phi}_{N/M}|}\approx\cot\Delta\theta_V|1+R^{\omega}_{N/M}|, \qquad (1)$$

where $R^{\omega,\phi}_{N/M}$ are the ratios of nucleon and meson-exchange amplitudes. Thus, one can get immediately an enhancement (suppression) of $R_{\omega/\phi}$, as compared to the OZI rule prediction, for a constructive (destructive) interference between the two ω amplitudes and for $|R^{\phi}_{N/M}|\ll|R^{\omega}_{N/M}|<1$. In our previous study [12] of ϕ production we supposed a destructive interference between meson-exchange and nucleon terms. Assuming the same for ω production, $R_{\omega/\phi}$ must decrease, even without any speculation on the strangeness content in the nucleon. In case of considering the ω production, however, this two-component model is not longer adequate, since one has to include various strong resonance channels. The ratio $R^{\omega}_{(N+N^*)/M}$ becomes complex, which may change the above estimates in any direction.

The resonance contribution to vector-meson production has its own interest because it might significantly affect in-medium polarization operators and the corresponding dilepton emissivity of hadronic matter [13–15]. Therefore its detailed study in elementary πN processes is another objective of the present work. An important step in this direction has been done recently by Riska and Brown in [16], where the relevant πNN^*, ωNN^*, and ϕNN^* coupling constants are expressed in terms of the corresponding couplings to nucleons using a quark model. Our study here exploits essentially the findings of [16]. The role of the low-lying nucleon resonances in a combined study of ρ^0 and ω production based on the relativistic coupled-channel model has been studied in Refs. [14,17]. Some aspects of the ρ meson spectral function in the nucleon-resonance model have been discussed in [18]. The contribution of the higher resonances to the ω photoproduction has been analyzed in Ref. [19].

Our analysis of the reaction $\pi N\to VN$ is based on calculations of the diagrams in Fig. 1. While the diagrams in Fig. 1 look like usual Feynman diagrams it should be stressed that they give a guidance of how to obtain from an effective interaction Lagrangian of hadronic fields a covariant parametrization of observables in strict tree level approximation. The pure t channel process in Fig. 1(a) is found to be insufficient to describe the data, even in a narrow interval of excess energies above the threshold. Therefore, we follow the common practice (cf. [19,20]) and include the s and u channels, which necessarily also contain baryon resonances. Additional ingredients are needed to achieve an accurate description of data within such a framework. In particular, the vertices needs to be dressed by form factors. The early theoretical studies [21,22] show, indeed, that predictions for hadronic observables are very sensitive to the parameters of the form factors, which cannot be fixed unambiguously without adjustments relying on the corresponding experimental data.

In Refs. [23,24] the parameters of VNN interactions have been determined by analyzing commonly the reactions $pp\to pp\omega$ and $pp\to pp\phi$ and the corresponding new DISTO data [25] at a given beam energy, assuming the same production mechanism without resonance contributions. In a previous paper [12], in order to constrain the parameter space further, we performed a combined analysis of the reactions $\pi^- p\to n\phi$ and $pp\to pp\phi$ at the same energy excess. A good description of available data has been achieved. We did not consider in [12] the ω production for which the production mechanism is more complicated because of the resonance contributions shown in Fig. 1(b). Therefore, the problem of the validity of the OZI rule was beyond the scope of considerations in [12].

In this paper we attempt a different approach with the goal to check the validity of the OZI rule in a combined study of the related reactions $\pi N\to N\omega$ and $\pi N\to N\phi$ using the known data within the same interval of excess energies 10–100 MeV and taking into account the nucleon resonance channels.

Our paper is organized as follows. In Sec. II, we define the effective Lagrangians, derive expressions for the amplitudes of the processes shown in Fig. 1 and discuss the parameter fixing. In Sec. III the results of numerical calculations and predictions are presented. A summary is given in Sec. IV.

II. AMPLITUDES

The differential cross section of the reaction $\pi^- p\to Vn$ with $V=\omega,\phi$ (cf. Fig. 1) has the obvious form in standard notation,

$$\frac{d\sigma}{d\Omega}=\frac{1}{64\pi^2 s}\frac{|\mathbf{q}|}{|\mathbf{k}|}|T|^2, \qquad (2)$$

where $k=(E_\pi,\mathbf{k})$ and $q=(E_V,\mathbf{q})$ are the four-momenta of the pion and the vector meson in the center of mass system (c.m.s.); the squared invariant amplitude $|T|^2$ includes the average and sum over the initial and final spin states, respectively. We denote the four-momenta of the initial (target) and final (recoil) nucleons by p and p', Ω and θ are the solid and polar angles of the produced vector meson in the c.m.s., $s=(p+k)^2$ is the usual Mandelstam variable.

We also consider the spin density matrix $\rho_{rr'}$, which defines the angular distribution in the decays [26] $\omega,\phi\to e^+e^-$, $\omega\to\pi^+\pi^-\pi^0$, and $\phi\to K^+K^-$. It has a simple form in the system where the vector meson is at rest (for details see [12]). The decay angles Θ and Φ are defined as polar and azimuthal angles of the direction of the three-momentum of one of the decay particles in the vector meson's rest frame. For the $\omega\to\pi^+\pi^-\pi^0$ decay, Θ is the polar angle of the direction of the vector product $(\boldsymbol{k}_{\pi^+}\times\boldsymbol{k}_{\pi^-})$, where $\boldsymbol{k}_{\pi^+}$ and $\boldsymbol{k}_{\pi^-}$ are the momenta of π^+ and π^- mesons, respectively [27]. The e^+e^- decay distribution integrated

over the azimuthal angle Φ, $\mathcal{W}(\cos\Theta)$, depends only on the diagonal matrix elements ρ_{00}, $\rho_{11}=\rho_{-1-1}$, normalized as $\rho_{00}+2\rho_{11}=1$, according to

$$\mathcal{W}^{e^+e^-}(\cos\Theta)=\frac{3}{4}[1+\rho_{00}+(1-3\rho_{00})\cos^2\Theta]. \quad (3)$$

The corresponding distributions for the hadronic decays $\phi\to K^+K^-$, $\omega\to\pi^+\pi^-\pi^0$ are

$$\mathcal{W}^h(\cos\Theta)=\frac{3}{2}[1-\rho_{00}-(1-3\rho_{00})\cos^2\Theta]. \quad (4)$$

In our calculation we choose the quantization axis **z** along the beam momentum.

A. Effective Lagrangians

In calculating the invariant amplitudes for the basic processes shown in Fig. 1 we use the following effective interaction Lagrangians.

(i) Interactions in the meson-exchange process [Fig. 1(a)]

$$\mathcal{L}_{V\rho\pi}=g_{V\rho\pi}\epsilon^{\mu\nu\alpha\beta}\partial_\mu^{(V)}V_\nu \mathrm{Tr}(\partial_\alpha\rho_\beta\pi), \quad (5)$$

$$\mathcal{L}_{\rho NN}=-g_{\rho NN}\bar{\psi}_N\left(\gamma_\mu-\frac{\kappa_{\rho NN}}{2M_N}\sigma_{\mu\nu}\partial_{(\rho)}^\nu\right)\rho^\mu\psi_N, \quad (6)$$

where $\mathrm{Tr}(\rho\pi)=\rho^0\pi^0+\rho^+\pi^-+\rho^-\pi^+$, and π and ρ^μ denote the pion and rho meson fields. The partial derivatives $\partial_\mu^{(V)}$ and $\partial_{(\rho)}^\nu$ are meant to act only on the corresponding fields V^μ and ρ^μ; $\epsilon_{\mu\nu\alpha\beta}$ is the Levi-Civita symbol with $\epsilon_{0123}=1$.

(ii) Interactions in the baryonic channels [Fig. 1(b)]

$$\mathcal{L}_{MNN}^{N_{1/2^+}(940)N}=\bar{\psi}_N\left[-\frac{f_{\pi NN}}{m_\pi}\gamma_5\gamma_\mu\partial^\mu\boldsymbol{\pi}\cdot\boldsymbol{\tau}-g_{VNN}\left(\gamma_\mu-\frac{\kappa_{VNN}}{2M_N}\sigma_{\mu\nu}\partial^\nu\right)V^\mu\right]\psi_N, \quad (7)$$

$$\mathcal{L}_{MNN^*}^{N_{1/2^+}(1440)P_{11}}=\bar{\psi}_N\left[-\frac{f_{\pi NN^*}^{1440}}{m_\pi}\gamma_5\gamma_\mu\partial^\mu\boldsymbol{\pi}\cdot\boldsymbol{\tau}-g_{VNN^*}^{1440}(\gamma_\mu+\partial_\mu\not{b}m_V^{-2})V^\mu\right]\psi_{N^*}+\mathrm{H.c.}, \quad (8)$$

$$\mathcal{L}_{MNN^*}^{N_{3/2^-}(1520)D_{13}}=\bar{\psi}_N\left[i\frac{f_{\pi NN^*}^{1520}}{m_\pi}\gamma_5\partial^\alpha\boldsymbol{\pi}\cdot\boldsymbol{\tau}+\frac{g_{VNN^*}^{1520}}{m_V^2}\sigma_{\mu\nu}\partial^\nu\partial^\alpha V^\mu\right]\psi_{N^*\alpha}+\mathrm{H.c.}, \quad (9)$$

$$\mathcal{L}_{MNN^*}^{N_{\frac{1}{2}^-}(1535)S_{11}}=\bar{\psi}_N\left[-\frac{f_{\pi NN^*}^{1535}}{m_\pi}\gamma_\mu\partial^\mu\boldsymbol{\pi}\cdot\boldsymbol{\tau}-g_{VNN^*}^{1535}\times\gamma_5(\gamma_\mu+\partial_\mu\not{b}m_V^{-2})V^\mu\right]\psi_{N^*}+\mathrm{H.c.}, \quad (10)$$

$$\mathcal{L}_{MNN^*}^{N_{1/2^-}(1650)S_{11}}=\bar{\psi}_N\left[-\frac{f_{\pi NN^*}^{1650}}{m_\pi}\gamma_\mu\partial^\mu\boldsymbol{\pi}\cdot\boldsymbol{\tau}-g_{VNN^*}^{1650}\times\gamma_5(\gamma_\mu+\partial_\mu\not{b}m_V^{-2})V^\mu\right]\psi_{N^*}+\mathrm{H.c.}, \quad (11)$$

$$\mathcal{L}_{MNN^*}^{N_{5/2^-}(1675)D_{15}}=\bar{\psi}_N\left[-\frac{f_{\pi NN^*}^{1675}}{m_\pi^2}\partial^\alpha\partial^\beta\boldsymbol{\pi}\cdot\boldsymbol{\tau}+\frac{g_{VNN^*}^{1675}}{m_V^2}\epsilon^{\alpha\gamma\mu\nu}\gamma_\nu\partial_\gamma\partial^\beta V_\mu\right]\psi_{N^*\alpha\beta}+\mathrm{H.c.}, \quad (12)$$

$$\mathcal{L}_{MNN^*}^{N_{\frac{5}{2}^+}(1680)F_{15}}=\bar{\psi}_N\left[-i\frac{f_{\pi NN^*}^{1680}}{m_\pi^2}\gamma_5\partial^\alpha\partial^\beta\boldsymbol{\pi}\cdot\boldsymbol{\tau}+\frac{g_{VNN^*}^{1680}}{m_V^2}\times(\gamma_\mu+\partial_\mu\not{b}m_V^{-2})\partial^\alpha\partial^\beta V^\mu\right]\psi_{N^*\alpha\beta}+\mathrm{H.c.}, \quad (13)$$

$$\mathcal{L}_{MNN^*}^{N_{\frac{3}{2}^-}(1700)D_{13}}=\bar{\psi}_N\left[i\frac{f_{\pi NN^*}^{1700}}{m_\pi}\gamma_5\partial^\alpha\boldsymbol{\pi}\cdot\boldsymbol{\tau}+\frac{g_{VNN^*}^{1700}}{m_V^2}\sigma_{\mu\nu}\partial^\nu\partial^\alpha V^\mu\right]\psi_{N^*\alpha}+\mathrm{H.c.}, \quad (14)$$

$$\mathcal{L}_{MNN^*}^{N_{3/2^+}(1720)P_{13}}=\bar{\psi}_N\left[i\frac{f_{\pi NN^*}^{1720}}{m_\pi}\partial^\alpha\boldsymbol{\pi}\cdot\boldsymbol{\tau}-\frac{g_{VNN^*}^{1720}}{M_{N^*}+M_N}\gamma_5\times(\gamma_\mu\partial^\alpha-g_\mu^\alpha\not{\partial})V^\mu\right]\psi_{N^*\alpha}+\mathrm{H.c.}, \quad (15)$$

where $\boldsymbol{\pi}$, V_μ, ψ_N, and ψ_{N^*} are the pion isovector, isoscalar vector meson $V=\omega,\phi$, nucleon, and Rarita-Schwinger nucleon-resonance field operators, respectively, and the subscript M stands for "meson;" $\boldsymbol{\tau}$ denotes the Pauli matrix. Note that these interaction Lagrangians do not contain partial derivatives of the fields $\psi_{\ldots}$ and their adjoints $\bar{\psi}_{\ldots}$. The notation of the masses is self-explanatory. We use the convention of Bjorken and Drell [28] in the definitions of γ matrices and the spin matrix $\sigma_{\mu\nu}$. The expressions Eqs. (7)–

(15) are based on [16].[1] As in [16] we include here all **** resonances up to 1720 MeV according to [2] and the *** resonance $N_{3/2^-}(1700)D_{13}$ as well. The contribution of the *** resonance $N_{1/2^+}(1710)P_{13}$ will be discussed below.

All coupling constants in t channel processes with off-shell mesons are dressed by monopole form factors [29] $F_i=(\Lambda_i^2-m_i^2)/(\Lambda_i^2-k_i^2)$, where k_i is the four-momentum of the exchanged meson. Following the scheme of the meson photoproduction in [30] we assume that the VNN and VNN^* vertices in s and u channel processes must also be dressed by form factors for off-shell baryons

$$F_B(r^2)=\frac{\Lambda_B^4}{\Lambda_B^4+(r^2-M_B^2)^2}, \tag{16}$$

where M_B is the baryon mass and r^2 stands for the four-momentum squared of the virtual baryons $B=N,N^*$ in Fig. 1(b). Equation (16) represents the simplest form, being symmetric in the s and u channels. (For a recent discussion of the structure of form factors cf. [31].) Both form factors are positive and decrease with increasing off-shellness.

B. Invariant amplitudes

The total invariant amplitude is the sum of the meson-exchange, nucleon, and nucleon-resonance channels,

$$T_\lambda=T_\lambda^{(M)}+T_\lambda^{(N)}+T_\lambda^{(N^*)}, \tag{17}$$

where $\lambda=0,\pm1$ is the polarization projection of the produced vector meson. The amplitude for the meson exchange-channel in Fig. 1(a) reads

$$T_\lambda^{(M)}=K^{\pi N}\epsilon^{\alpha\beta\gamma\delta}[\bar{u}(p')\Gamma_\delta^{(\rho)}(k_{(\rho)})u(p)]q_\alpha k_\gamma \varepsilon_\beta^{*\lambda} I_\pi, \tag{18}$$

where

$$\Gamma_\alpha^{(\rho)}(k_{(\rho)})=\gamma_\alpha+i\frac{\kappa_{\rho NN}}{2M_N}\sigma_{\alpha\beta}k_{(\rho)}^\beta, \tag{19}$$

$$K^{\pi N}(k_{(\rho)})=-\frac{g_{\rho NN}g_{V\rho\pi}}{k_{(\rho)}^2-m_\rho^2}\frac{\Lambda_{\rho NN}^2-m_\rho^2}{\Lambda_{\rho NN}^2-k_{(\rho)}^2}\frac{\Lambda_{V\rho\pi}^{\rho 2}-m_\rho^2}{\Lambda_{V\rho\pi}^{\rho 2}-k_{(\rho)}^2} \tag{20}$$

with $k_{(\rho)}=p'-p$ as the virtual ρ meson's four-momentum, $\varepsilon_\beta^\lambda$ is the vector meson's polarization four-vector, I_π denotes the isospin factor being $\sqrt{2}$ (1) for a π^- (π^0) meson in the entrance channel, the nucleon spin indices are not displayed, α, β, γ, δ, μ, ν, τ are Lorentz indices throughout the paper (not to be confused with the notations of the meson species π, ρ, ω, ϕ), and $u(p)$ denotes bispinors (not to be confused with the Mandelstam variable u).

[1]Our notation differs from that in [16] by the substitutions $\partial\to i\partial$ and $ig_{VNN}\to -g_{VNN}$ keeping the relative phases between $f_{\pi NN}$ and $f_{\pi NN^*}$ and g_{VNN} and g_{VNN^*} the same as in [16]. We also express $\mathcal{L}_{MNN^*}$ in a manifestly gauge-invariant form.

The invariant amplitudes for the nucleon and nucleon-resonance channels in Fig. 1(b) have the following form:

$$T_\lambda^{(N)}=g_{VNN}\frac{f_{\pi NN}}{m_\pi}\bar{u}(p')\mathcal{A}^\mu(N)u(p)\varepsilon_\mu^{*\lambda}I_\pi, \tag{21}$$

$$T_\lambda^{(N^*)}=g_{VNN^*}\frac{f_{\pi NN^*}}{m_\pi}\bar{u}(p')\mathcal{A}^\mu(N^*)u(p)\varepsilon_\mu^{*\lambda}I_\pi, \tag{22}$$

where the operators $\mathcal{A}_\mu(N)$ and $\mathcal{A}_\mu(N^*)$ follow from the effective Lagrangians of Eqs. (7)–(15) as

$$\mathcal{A}_\mu(N^{940})=-i\frac{\Gamma_\mu^V(-q)\Lambda(p_L,M_{N^*})\gamma_5 \not{k} F_N(s)}{s-m_N^2} - i\frac{\gamma_5\not{k}\Lambda(p_R,M_{N^*})\Gamma_\mu^V(-q)F_N(u)}{u-m_N^2}, \tag{23}$$

$$\mathcal{A}_\mu(N^{1440})=-i\frac{\gamma_\mu\Lambda(p_L,M_{N^*})\gamma_5\not{k}F_{N^*}(s)}{s-M_{N^*}^2+i\Gamma_{N^*}M_{N^*}} - i\frac{\gamma_5\not{k}\Lambda(p_R,M_{N^*})\gamma_\mu F_{N^*}(u)}{u-M_{N^*}^2+i\Gamma_{N^*}M_{N^*}}, \tag{24}$$

$$\mathcal{A}_\mu(N^{1520})=-\frac{\sigma_{\mu\nu}q^\nu q^\alpha\Lambda_{\alpha\beta}(p_L,M_{N^*})\gamma_5 k^\beta F_{N^*}(s)}{m_V^2(s-M_{N^*}^2+i\Gamma_{N^*}M_{N^*})} - \frac{\gamma_5 k^\alpha\Lambda_{\alpha\beta}(p_R,M_{N^*})\sigma_{\mu\nu}q^\nu q^\beta F_{N^*}(u)}{m_V^2(u-M_{N^*}^2+i\Gamma_{N^*}M_{N^*})}, \tag{25}$$

$$\mathcal{A}_\mu(N^{1535})=-i\frac{\gamma_5\gamma_\mu\Lambda(p_L,M_{N^*})\not{k}F_{N^*}(s)}{s-M_{N^*}^2+i\Gamma_{N^*}M_{N^*}} - i\frac{\not{k}\Lambda(p_R,M_{N^*})\gamma_5\gamma_\mu F_{N^*}(u)}{u-M_{N^*}^2+i\Gamma_{N^*}M_{N^*}}, \tag{26}$$

$$\mathcal{A}_\mu(N^{1650})=-i\frac{\gamma_5\gamma_\mu\Lambda(p_L,M_{N^*})\not{k}F_{N^*}(s)}{s-M_{N^*}^2+i\Gamma_{N^*}M_{N^*}} - i\frac{\not{k}\Lambda(p_R,M_{N^*})\gamma_5\gamma_\mu F_{N^*}(u)}{u-M_{N^*}^2+i\Gamma_{N^*}M_{N^*}}, \tag{27}$$

$$\mathcal{A}_\mu(N^{1675})=-\frac{\epsilon_{\tau\mu\nu}^\alpha q^\tau q^\beta k^\gamma k^\delta}{m_\pi m_V^2}\left(\frac{\gamma^\nu\Lambda_{\alpha\beta,\gamma\delta}(p_L,M_{N^*})F_{N^*}(s)}{s-M_{N^*}^2+i\Gamma_{N^*}M_{N^*}} + \frac{\Lambda_{\gamma\delta,\alpha\beta}(p_R,M_{N^*})\gamma^\nu F_{N^*}(u)}{u-M_{N^*}^2+i\Gamma_{N^*}M_{N^*}}\right), \tag{28}$$

$$\mathcal{A}_\mu(N^{1680}) = -i\frac{q^\alpha q^\beta k^\gamma k^\delta}{m_\pi m_V^2}\left(\frac{\gamma_\mu \Lambda_{\alpha\beta,\gamma\delta}(p_L,M_{N*})\gamma_5 F_{N*}(s)}{s-M_{N*}^2+i\Gamma_{N*}M_{N*}} + \frac{\gamma_5 \Lambda_{\gamma\delta,\alpha\beta}(p_R,M_{N*})F_{N*}(u)}{u-M_{N*}^2+i\Gamma_{N*}M_{N*}}\right), \tag{29}$$

$$\mathcal{A}_\mu(N^{1700}) = -\frac{\sigma_{\mu\nu}q^\nu q^\alpha \Lambda_{\alpha\beta}(p_L,M_{N*})\gamma_5 k^\beta F_{N*}(s)}{m_V^2(s-M_{N*}^2+i\Gamma_{N*}M_{N*})} - \frac{\gamma_5 k^\alpha \Lambda_{\alpha\beta}(p_R,M_{N*})\sigma_{\mu\nu}q^\nu q^\beta F_{N*}(u)}{m_V^2(u-M_{N*}^2+i\Gamma_{N*}M_{N*})}, \tag{30}$$

$$\mathcal{A}_\mu(N^{1720}) = -i\frac{\gamma_5(q^\alpha\gamma_\mu - g_\mu^\alpha \not{q})\Lambda_{\alpha\beta}(p_L,M_{N*})k^\beta F_{N*}(s)}{(M_{N*}+M_N)(s-M_{N*}^2+i\Gamma_{N*}M_{N*})} - i\frac{k^\beta \Lambda_{\beta\alpha}(p_R,M_{N*})\gamma_5(q^\alpha\gamma_\mu - g_\mu^\alpha \not{q})F_{N*}(u)}{(M_{N*}+M_N)(u-M_{N*}^2+i\Gamma_{N*}M_{N*})}, \tag{31}$$

with $p_L=p+k$, $p_R=p-q$, and Γ_μ^V as in Eq. (19) but with κ_{VNN}.

The resonance propagators in Eqs. (24)–(31) are defined by the conventional method [32] assuming the validity of the spectral decomposition

$$\psi_{N*}(x) = \int \frac{d^3\mathbf{p}}{(2\pi)^3\sqrt{2E_p}}[a_{\mathbf{p},r}u_{N*}^r(p)e^{-ipx} + b_{\mathbf{p},r}^+ v_{N*}^r(p)e^{+ipx}]. \tag{32}$$

The finite decay width Γ_{N*} is introduced into the propagator denominators by substituting $M_{N*}\to M_{N*}-i/2\Gamma_{N*}$. Therefore, the operators $\Lambda(p,M)$ are defined as

$$\Lambda(p,M) = \frac{1}{2}\sum_r\left(\left[1+\frac{p_0}{E_0}\right]u^r(\mathbf{p},E_0)\otimes\overline{u^r}(\mathbf{p},E_0) - \left[1-\frac{p_0}{E_0}\right]v^r(-\mathbf{p},E_0)\otimes\overline{v^r}(-\mathbf{p},E_0)\right) = \not{p}+M, \tag{33}$$

$$\Lambda_{\alpha\beta}(p,M) = \frac{1}{2}\sum_r\left(\left[1+\frac{p_0}{E_0}\right]\mathcal{U}_\alpha^r(\mathbf{p},E_0)\otimes\overline{\mathcal{U}_\beta^r}(\mathbf{p},E_0) - \left[1-\frac{p_0}{E_0}\right]\mathcal{V}_\alpha^r(-\mathbf{p},E_0)\otimes\overline{\mathcal{V}_\beta^r}(-\mathbf{p},E_0)\right), \tag{34}$$

$$\Lambda_{\alpha\beta,\gamma\delta}(p,M) = \frac{1}{2}\sum_r\left(\left[1+\frac{p_0}{E_0}\right]\mathcal{U}_{\alpha\beta}^r(\mathbf{p},E_0)\otimes\overline{\mathcal{U}_{\gamma\delta}^r}(\mathbf{p},E_0) - \left[1-\frac{p_0}{E_0}\right]\mathcal{V}_{\alpha\beta}^r(-\mathbf{p},E_0)\otimes\overline{\mathcal{V}_{\gamma\delta}^r}(-\mathbf{p},E_0)\right), \tag{35}$$

where $E_0=\sqrt{\mathbf{p}^2+M^2}$ and the Rarita-Schwinger spinors read

$$\mathcal{U}_\alpha^r(p) = \sum_{\lambda,s}\left\langle 1\lambda\,\frac{1}{2}s\middle|\frac{3}{2}r\right\rangle\varepsilon_\alpha^\lambda(p)u^s(p), \tag{36}$$

$$\mathcal{U}_{\alpha\beta}^r(p) = \sum_{\lambda,\lambda' s,t}\left\langle 1\lambda\,\frac{1}{2}s\middle|\frac{3}{2}t\right\rangle\left\langle\frac{3}{2}t1\lambda'\middle|\frac{5}{2}r\right\rangle \times\varepsilon_\alpha^\lambda(p)\varepsilon_\beta^{\lambda'}(p)u^s(p). \tag{37}$$

The spinors v and $\mathcal{V}$ are related to u and $\mathcal{U}$ as $v(p)=i\gamma_2 u^*(p)$ and $\mathcal{V}(p)=i\gamma_2\mathcal{U}^*(p)$, respectively. Note that our choice of the spin-projection operators $\Lambda(p,M)$ for spin-$\frac{3}{2}$ and spin-$\frac{5}{2}$ off-shell baryons is different from the commonly used on-shell operator [13,33], but coincides with the latter one at $p^2=M^2$. We discuss this difference in Appendix A.

The polarization four-vector of a spin-1 particle with spin projection λ, four-momentum $p=(E,\mathbf{p})$, and mass m_V reads

$$\varepsilon^\lambda(p) = \left(\frac{\boldsymbol{\epsilon}^\lambda\cdot\mathbf{p}}{m_V}, \boldsymbol{\epsilon}^\lambda + \frac{\mathbf{p}(\boldsymbol{\epsilon}^\lambda\cdot\mathbf{p})}{m_V(E+m_V)}\right), \tag{38}$$

where the three-dimensional polarization vector $\boldsymbol{\epsilon}$ is defined as

$$\boldsymbol{\epsilon}^{\pm1} = \mp\frac{1}{\sqrt{2}}(1,\pm i,0), \quad \boldsymbol{\epsilon}^0=(0,0,1). \tag{39}$$

In our calculations we use energy-dependent total resonance decay widths Γ_{N*}. However, taking into account that the effect of a finite width is quite different for s and u channels, because of the evident relation $|u|+M_{N*}^2 \gg |s-M_{N*}^2|$, we use $\Gamma_{N*}=\Gamma_{N*}^0$ for the u channels. For the s channels the energy-dependent widths are calculated according to Ref. [34]; the relevant equations are listed in Appendix B.

C. Fixing parameters

The coupling constant $g_{\phi\rho\pi}$ is determined by the $\phi\to\rho\pi$ decay. The value $\Gamma_{\phi\to\rho\pi}=0.69$ MeV [2] results in $|g_{\phi\rho\pi}|=1.1$ GeV^{-1}. The ratio $R_{\omega/\phi}=g_{\omega\rho\pi}/g_{\phi\rho\pi}=12.9$ is evaluated in a simultaneous analysis of the $\omega\to\pi\gamma$ and $\phi\to\pi\gamma$ decays and by applying the vector dominance model [9]. This value is consistent with the standard OZI rule violation and results in $|g_{\omega\rho\pi}|=|12.9 g_{\phi\rho\pi}|=14.19$ GeV^{-1}. Note that the analysis of the $pp\to pp\omega(\phi)$ reaction within a two-component model (without baryon resonances) in [24] favors a sizable deviation of $R_{\omega/\phi}$ from the OZI ratio. Some

other (different) estimates of $g_{\omega\rho\pi}$, which lead to a violation of the OZI rule, are also discussed in [9].

The sign of $g_{\omega\rho\pi}$ is yet unknown, however, the study of π photoproduction [35] points to a positive value, which we use in our subsequent calculations as a preferred choice, i.e., $g_{\omega\rho\pi}=14.9\ \mathrm{GeV}^{-1}$. The SU(3) symmetry considerations in [24,36] predict an opposite sign for $g_{\phi\rho\pi}$; thus $g_{\phi\rho\pi}=-1.1\ \mathrm{GeV}^{-1}$. To explore the sensitivity of the results to the above choice of the signs of the couplings, we shall later on also discuss the case of opposite signs, namely $g_{\omega\rho\pi}<0$ and $g_{\phi\rho\pi}>0$.

The remaining parameters of the meson-exchange amplitude for the process in Fig. 1(a) are taken from the Bonn model as listed in Table B.1 (Model II) of Ref. [29]: $g_{\rho NN}=3.72$, $\kappa_{\rho NN}=6.1$, and $\Lambda_{\rho NN}=1.3$. The parameter $\Lambda^{\rho}_{V\rho\pi}$ will be determined later.

The nucleon and nucleon-resonance amplitudes in Fig. 1(b) and Eqs. (23)–(31) are determined by the couplings $f_{\pi NN}$, $f_{\pi NN*}$, $g_{\omega NN}$, $g_{\omega NN*}$, $g_{\phi NN}$, $g_{\phi NN*}$, $g_{VNN}\kappa_{VNN}$, the resonance widths Γ^{0}_{N*}, the branching ratios B^{π}_{N*}, and the cutoffs Λ_B. For the coupling constant $f_{\pi NN}$ we use the standard value $f_{\pi NN}=1.0$ [16,29]. For the ωNN coupling, we use the value $g_{\omega NN}=10.35$ determined recently [37] by fitting nucleon-nucleon scattering data. This value as well as $\kappa_{\omega NN}=0$ is close to that which has been found in a study of πN scattering and the reaction $\gamma N\to\pi N$ [35].

The values of coupling constants $f_{\pi NN*}$ are determined by a comparison of calculated $N^*\to N\pi$ decay widths with experimental values [2]. The corresponding equations read [16]

$$\Gamma^{N_{1/2^\pm}}_{N^*\to N\pi}=\frac{3f^2_{\pi NN*}k}{4\pi m^2_\pi}\frac{(E_{p'}\mp M_N)(M_{N*}\pm M_N)^2}{M_{N*}}, \quad (40)$$

$$\Gamma^{N_{3/2^\pm}}_{N^*\to N\pi}=\frac{f^2_{\pi NN*}k^3}{4\pi m^2_\pi}\frac{(E_{p'}\pm M_N)}{M_{N*}}, \quad (41)$$

$$\Gamma^{N_{5/2^\pm}}_{N^*\to N\pi}=\frac{f^2_{\pi NN*}k^5}{10\pi m^2_\pi}\frac{(E_{p'}\mp M_N)}{M_{N*}}. \quad (42)$$

The values of $f_{\pi NN*}$ calculated from these expressions are listed in Table I. The corresponding signs are taken in accordance with the quark model prediction of Ref. [16]. The numbers in parentheses in Table I are the values from the quark model [16]. One can see that most of them are close to the values extracted from the data. The strongest deviations appear for $N_{5/2^+}(1680)F_{15}$ and $N_{3/2^+}(1720)P_{13}$, which, however, deliver only subleading contributions.

The coupling constants $g_{\omega NN*}$ cannot be found by this method because the corresponding decays are below threshold. Therefore, they are determined by $g_{\omega NN*}=(g_{\omega NN*}/g_{\omega NN})g_{\omega NN}$, where the ratio $(g_{\omega NN*}/g_{\omega NN})$ is determined by the quark model calculation of Ref. [16]. We show them in Table I too, where, for convenience, we also present decay widths, and branching ratios used in our calculations. Note that the masses, decay widths and branching ratios in Table I represent the averages in [2]. Slightly different values have been extracted in [38] in a recent reanalysis of the data.

TABLE I. Parameters for the resonance masses, coupling constants, total decay widths, and branching ratios for $N^*\to N\pi$ decays. The numbers in parentheses are from the quark model [16]. The resonance masses and decay widths are in units of MeV.

Baryon	M_{N*}	$f_{\pi NN*}$	$g_{\omega NN*}$	Γ^0_{N*}	B^π_{N*}
$N_{1/2^+}N$	940	1.0	10.35		
$N_{1/2^+}P_{11}$	1440	0.39 (0.26)	6.34	350	0.65
$N_{3/2^-}D_{13}$	1520	−1.56 (−1.71)	8.88	120	0.55
$N_{1/2^-}S_{11}$	1535	0.36 (0.49)	−5.12	150	0.50
$N_{1/2^-}S_{11}$	1650	0.31 (0.28)	2.56	150	0.71
$N_{5/2^-}D_{15}$	1675	0.10 (0.09)	10.87	150	0.45
$N_{5/2^+}F_{15}$	1680	−0.42 (−0.12)	−14.07	130	0.65
$N_{3/2^-}D_{13}$	1700	0.36 (0.22)	2.81	100	0.10
$N_{3/2^+}P_{13}$	1720	−0.25 (−1.05)	−3.17	150	0.15

The couplings ϕNN, $\phi NN*$ determined by SU(3) symmetry considerations are

$$g_{\phi NN}=-\tan\Delta\theta_V g_{\omega NN}, \quad g_{\phi NN*}=-\tan\Delta\theta_V g_{\omega NN*}, \quad (43)$$

where $\Delta\theta_V$ is the above quoted deviation from the ideal ω-ϕ mixing. Similarly, we assume $g_{\phi NN}\kappa_{\phi NN}\simeq-\tan\Delta\theta_V g_{\omega NN}\kappa_{\omega NN}=0$, or $\kappa_{\phi NN}\simeq 0$, which is consistent with the estimate in [39]. Thus, we use for definiteness the relative phase of coupling constants to be real according to our experience of calculating meson photoproduction and the symmetry of the quark model. (In some sense our amplitudes can be considered as the Born terms for further multichannel analyses, such as in [35,40,41], where some effective imaginary part of the form factors can be generated dynamically. Such a cumbersome analysis is beyond the scope of the present work; therefore, there is a phase uncertainty in the analysis, which, however, is not expected to affect the results noticeably.)

The yet undetermined parameters are the cutoff parameters $\Lambda^{\rho}_{\phi\rho\pi}$ and $\Lambda^{\rho}_{\omega\rho\pi}$ for the virtual ρ meson in the $V\rho\pi$ vertex, the cutoff Λ_N, and the eight cutoffs Λ_{N*} in Eq. (16). We can reduce the number of parameters by making the natural assumptions

$$\Lambda^{\rho}_{\phi\rho\pi}=\Lambda^{\rho}_{\omega\rho\pi}\equiv\Lambda^{\rho}_V, \quad (44)$$

$$\Lambda_B=\Lambda_{N^*_i}, \quad i=1,8. \quad (45)$$

Our best fit of the total cross sections of the existing data is obtained by $\Lambda^{\rho}_V=1.24$ GeV, $\Lambda_N=0.66$ GeV, and $\Lambda_B=0.85$ GeV.

It should be noted that our consideration does not include explicitly the final state interaction (FSI). A corresponding analysis of FSI in the reaction $\gamma p\to\omega p$ has been performed on the basis of distorted-wave Born approximation in Ref. [42]. A FSI correcting absorption factor is found as a flat function of the energy in a wide energy region from the

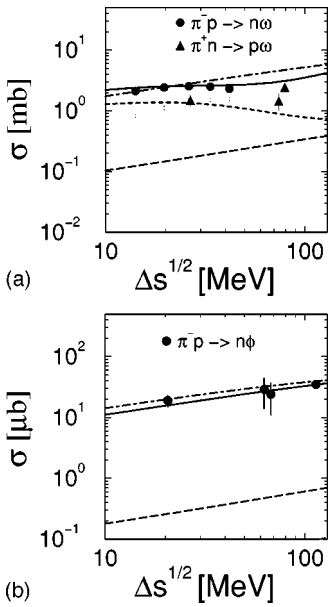

FIG. 2. Total cross sections for the reactions $\pi N \to N\omega$ (top panel) and $\pi^- p \to n\phi$ (bottom panel) as a function of the energy excess $\Delta s^{1/2}$. The meaning of the curves is meson exchange, dot-dashed; direct and crossed nucleon terms, long-dashed; N^* resonances, dashed; full amplitude, solid. Data from [43,44].

threshold up to few GeV. Therefore, since we focus on the very narrow region of 10–100 MeV excess energy, we can assume the FSI absorption factor as a constant that is included phenomenologically in the cutoff parameters. The same assumption holds for the initial state interaction. The sensitivity of the cross section on the cutoffs will be discussed below.

III. RESULTS

The results of our full calculation of the total cross sections as a function of the energy excess $\Delta s^{1/2} = \sqrt{s} - M_N - m_V$, including all amplitudes depicted in Fig. 1, are represented by the solid curves in Fig. 2. We also show separately the contributions of meson exchange, nucleon, and nucleon-resonance channels. The data for the reaction $\pi^- p \to \phi n$ are taken from Ref. [43], while the data for the reactions $\pi^+ n \to \omega p$ and $\pi^- p \to \omega n$ are from Refs. [43,44], respectively. Note that here we display the total cross section $\sigma_{\rm tot}$ of the reaction $\pi^- p \to \omega n$, which differs from the differential cross section $\sigma_{\rm dif}$ in Ref. [44] by a factor [9,45] included in the phase space of the unstable ω meson,

$$\sigma_{\rm tot} = \sigma_{\rm dif} \left\{ \int_{\sqrt{P_{\rm min}^2 + M_N^2}}^{\sqrt{P_{\rm max}^2 + M_N^2}} \sqrt{\frac{\lambda_f(s')\lambda_i(s)}{\lambda_f(s)\lambda_i(s')}} \times \frac{2\sqrt{s'}\Gamma_\omega m_\omega dE}{\pi[(m_\omega^2 - s' + 2\sqrt{s'}E - M_N^2)^2 + \Gamma_\omega^2 m_\omega^2]} \right\}^{-1}, \tag{46}$$

where $\sqrt{s'} = E + \sqrt{E^2 - M_N^2 + m_\omega^2}$, Γ_ω is the ω decay width, and $\lambda_i(s)[\lambda_f(s)] = \lambda(s, m_\pi^2, M_N^2)[\lambda(s, m_\omega^2, M_N^2)]$ with $\lambda(x,y,z) = (x-y-z)^2 - 4yz$. The intervals $[P_{\rm max}, P_{\rm min}]$ for given p' (or s) are as in [44].

From Fig. 2 (top panel) it is evident that the total amplitude of ω production is a result of strong interferences of all channels: the meson exchange (dot-dashed curve), the nucleon term (long dashed curve), and the resonance contribution (dashed curve) play a comparative role. For the ϕ production (cf. Fig. 2, bottom panel) only meson and nucleon terms are important. The resonance contribution is rather small and is, therefore, not displayed here. Moreover, the relative contribution of the nucleon term in ϕ production is much smaller than for ω production. That is because the initial energy $\sqrt{s} = M_N + m_V + \Delta s^{1/2}$ is greater for the ϕ production at the same energy excess and, as a consequence, we have two suppression factors: (i) the nucleon/resonance denominators and (ii) the form factors $F_{N,N*}$ in Eqs. (23)–(31). The interference of the meson-exchange and nucleon terms is almost destructive, while the contribution of the resonant part is more complicated because the amplitude is complex with different phases for different resonances.

The sensitivity of our calculations to the choice of cutoff parameters for the example of the reaction $\pi^- p \to \omega n$ is exhibited in Fig. 3 for the total cross section and individual channels. In the top panel we exhibit the dependence on Λ_V^ρ at fixed $\Lambda_B = 0.85$ GeV and $\Lambda_N = 0.66$ GeV, the dependence on Λ_B at fixed $\Lambda_V^\rho = 1.24$ GeV and $\Lambda_N = 0.66$ GeV is shown in the middle panel, and the dependence on Λ_N at fixed $\Lambda_V^\rho = 1.24$ GeV and $\Lambda_N = 0.85$ GeV is displayed in the bottom panel. One can see a noticeable dependence on Λ_V^ρ and a weaker dependence on Λ_B, Λ_N.

In order to illustrate the structure of the resonant part, we show in Fig. 4 the contribution of each resonance separately as a function of the ω production angle at two excess energies $\Delta s^{1/2} = 20$ (100) MeV in the top (bottom) panel. One can see that just near the threshold the resonances with $J = \frac{1}{2}$ are important. Together with the nucleon term, they are $N_{1/2^+}(1440)P_{11}$, $N_{1/2^-}(1535)S_{11}$, and $N_{1/2^-}(1650)S_{11}$. It is interesting that the separate contributions of the two latter ones are greater than the nucleon term. But their phases are opposite and, therefore, they cancel each other. The cancellation increases with energy, which results in a total decrease of the resonance contribution. On the other hand one can see that the relative role of the higher spin resonances with orbital/radial excitations, being proportional to $\mathbf{q}^2$ and $\mathbf{q}^4$, increases with increasing values of $\Delta s^{1/2}$, as illustrated in Fig. 5. This enhancement, however, is smaller than the effect of the strong destructive interference of the resonance amplitudes and, therefore, the total contribution of the resonance channel decreases with energy as shown in Fig. 2.

In our analyses we do not include the *** resonance $N_{1/2^+}(1710)P_{11}$ [2], as in [16]. A simple estimate shows that its contribution is rather small. Indeed, the calculation in [15], within the vector dominance model, shows that the ωNN^* coupling for $N_{1/2^+}(1710)P_{11}$ is about four times smaller than for the $N_{1/2^+}(1440)P_{11}$ resonance. Observing further that the corresponding pion decay width of

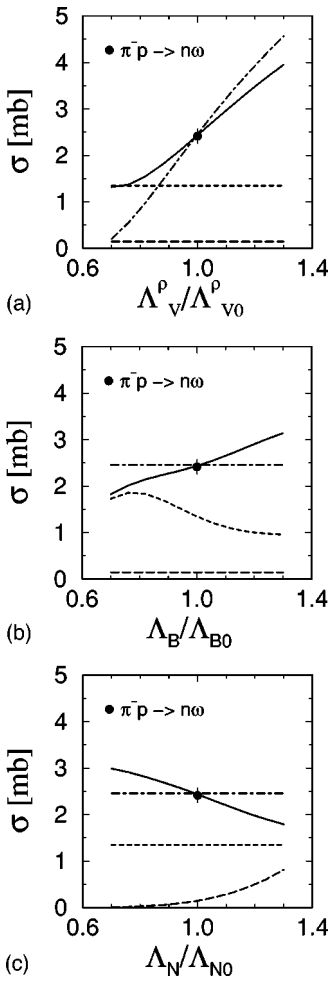

FIG. 3. Sensitivity of the total cross section for the reaction $\pi^- p \to n\omega$ on the cutoff parameters Λ_V^ρ, Λ_B, and Λ_N at $\Delta s^{1/2} = 20$ MeV. $\Lambda_{V0}^\rho = 1.24$ GeV, $\Lambda_{B0} = 0.85$ GeV, and $\Lambda_{N0} = 0.66$ GeV, respectively. Notation as in Fig. 2.

$N_{1/2+}(1710)P_{11}$, 5–15 MeV, is much smaller than that of $N_{1/2+}(1440)P_{11}$, 210–250 MeV, we can expect a negligible contribution of $N_{1/2+}(1710)P_{11}$, being about one order of magnitude smaller than that of $N_{1/2+}(1440)P_{11}$.

Figures 6 and 7 exhibit the angular distributions of the ω and ϕ production cross sections at $\Delta s^{1/2} = 20$ and 100 MeV, respectively. One can see that the destructive interference between meson-exchange and nucleon channels, which is stronger for backward production, results in a nonmonotonic angular distribution. The effect is stronger at $\Delta s^{1/2} = 100$ MeV.

Figure 8 (top panel) shows the ratio of the averaged amplitudes $|T_V|$ of ω and ϕ production as a function of the vector meson's production angle at $\Delta s^{1/2} = 20$ MeV. $|T_V|$ is defined by

$$|T_V| = \left[\sum_{m_i, m_f, \lambda} |T^V_{m_f, \lambda; m_i}|^2 \right]^{1/2}, \tag{47}$$

where m_i, m_f, and λ are the spin projections of the target, recoil protons, and vector meson, respectively. The short-

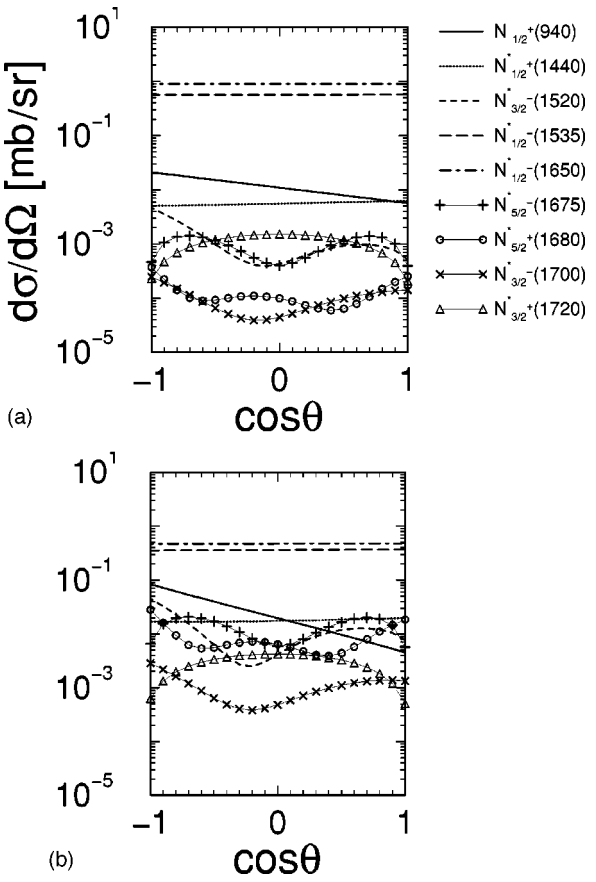

FIG. 4. Individual contributions of nucleon resonances listed in Table I to the angular differential cross section of ω production at $\Delta s^{1/2} = 20$ MeV (top panel) and 100 MeV (bottom panel).

dashed straight lines in Fig. 8 correspond to the standard OZI rule violation value $R^{OZI}_{\omega/\phi} = \cot \Delta\theta_V = 15.43$. The long-dashed curve corresponds to the ratio of pure nucleon channels taken separately, the dot-dashed curve is the result for a pure meson-exchange, while the solid line represents the full calculation. Note that the ratio even for pure meson-exchange amplitudes $R^{M}_{\omega/\phi}$ is smaller than $R^{OZI}_{\omega/\phi}$. This is because at the threshold,

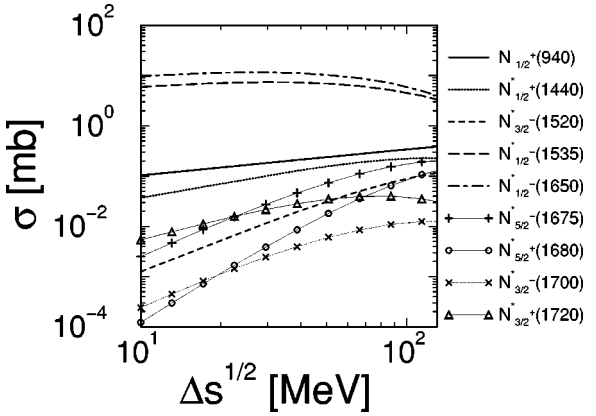

FIG. 5. Individual contributions of nucleon resonances listed in Table I to the total cross section of ω production as a function of $\Delta s^{1/2}$.

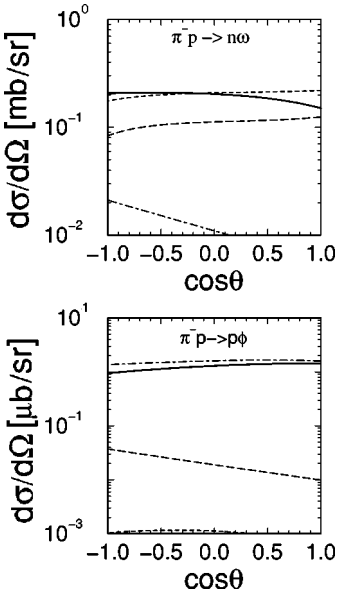

FIG. 6. Angular differential cross sections for the reactions $\pi^- p \to n\omega$ (top panel) and $\pi^- p \to n\phi$ (bottom panel) at $\Delta s^{1/2} = 20$ MeV. Notation as in Fig. 2.

$$R^M_{\omega/\phi} \simeq \frac{g_{\omega\rho\pi}}{g_{\phi\rho\pi}} \frac{m_\omega}{m_\phi} \frac{f(m_\omega)}{f(m_\phi)} \simeq 9.9 \frac{f(m_\omega)}{f(m_\phi)}, \tag{48}$$

where $f(m)$ is a smooth function of m. The ratio for pure resonance terms is greater than $R^{OZI}_{\omega/\phi}$ by an order of magnitude and more, i.e., $R^{N*}_{\omega/\phi} \sim 500(250)$ at $\theta = \pi(0)$, because of a strong propagator and form factor suppression for ϕ production. In the absence of the resonant amplitude, the destructive interference of meson-exchange (M) and nucleon (N) channels results in $R^{M+N}_{\omega/\phi} < R^M_{\omega/\phi}$. The presence of the resonance components leads to $R^M_{\omega/\phi} < R_{\omega/\phi} < R^{OZI}_{\omega/\phi}$.

Figure 8 (bottom panel) shows the ratio of the angular integrated amplitudes

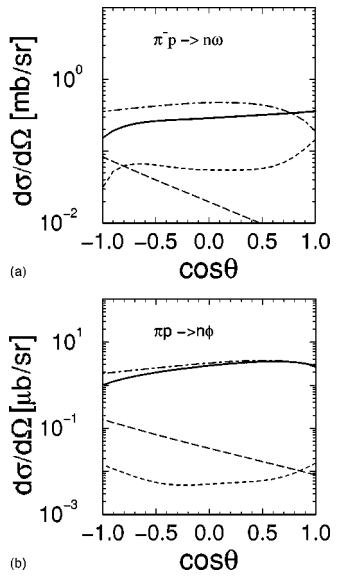

FIG. 7. As in Fig. 6 but at $\Delta s^{1/2} = 100$ MeV.

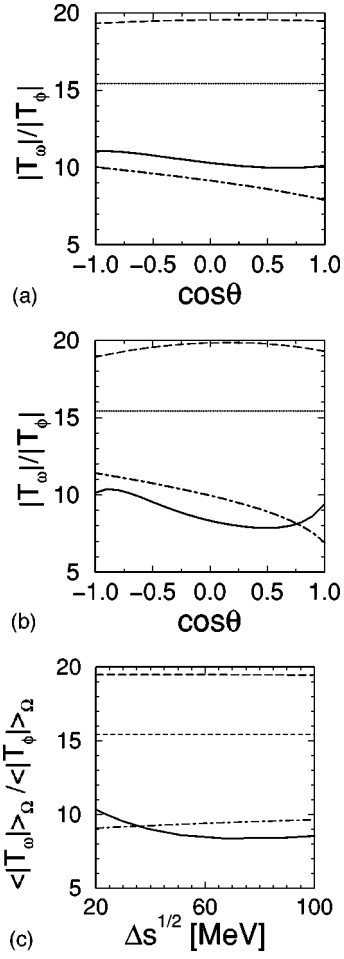

FIG. 8. Ratio of the amplitudes of ω and ϕ production. Top panel: the ratio as a function of $\cos\theta$ at $\Delta s^{1/2} = 20$ MeV, bottom panel: the ratio averaged over production angle as a function of $\Delta s^{1/2}$. Notation as in Fig. 2.

$$\langle |T_V| \rangle_\Omega = \left[\sum_{m_i, m_f, \lambda} \frac{1}{4\pi} \int d\Omega |T^V_{m_f, \lambda; m_i}|^2 \right]^{1/2} \tag{49}$$

of ω and ϕ production as a function of $\Delta s^{1/2}$. One can see that $R_{\omega/\phi}$ (solid curve) may be slightly above or below the pure $R^M_{\omega/\phi}$ value (dot-dashed curve), however, remaining much smaller than $R^{OZI}_{\omega/\phi}$, namely, $R_{\omega/\phi} = 7.5$–10, in agreement with the analysis in [9].

Figure 9 shows the results of our full calculation of the spin density matrix element ρ_{00} at $\Delta s^{1/2} = 20$ and 100 MeV in the top and bottom panels, respectively. Near the threshold, the meson-exchange amplitude behaves as

$$T^{(M)}_\lambda \sim \mathbf{k} \cdot [\mathbf{k} \times \boldsymbol{\epsilon}^{*\lambda}]. \tag{50}$$

That means that only $\lambda = \pm 1$ contributes and, therefore, ρ_{00} is suppressed. The pure nucleon s channel amplitude behaves as

$$T^{(N)}_\lambda \sim \langle f | \boldsymbol{\sigma} \cdot \boldsymbol{\epsilon}^{*\lambda} | i \rangle, \tag{51}$$

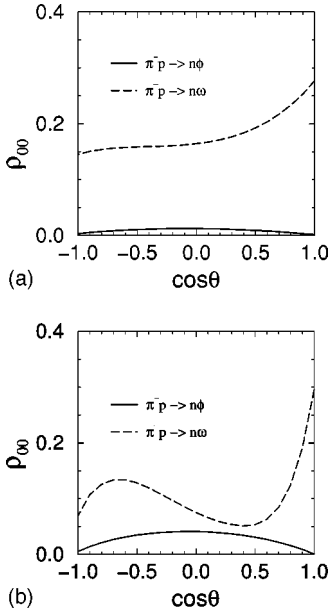

FIG. 9. Spin density matrix element ρ_{00} for ω and ϕ production as a function of $\cos\theta$ at $\Delta s^{1/2}=20$ MeV (top panel) and 100 MeV (bottom panel).

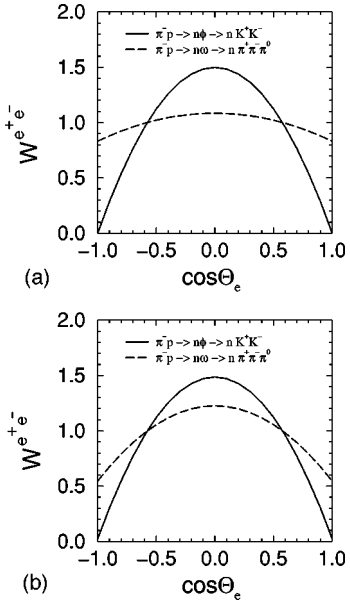

FIG. 10. Meson angular distributions in the reactions $\pi^- p \to n\phi \to nK^+K^-$ and $\pi^- p \to n\omega \to n\pi^+\pi^-\pi^0$ at $\Delta s^{1/2}=20$ MeV. Top panel: the distribution at forward vector-meson production angles, bottom panel: the distribution averaged over all production angles.

which results in an isotropic spin density, i.e., $\rho_{00}=\rho_{11}=\rho_{-1-1}=1/3$. The resonance amplitudes have additional terms proportional to $\mathbf{k}\cdot\boldsymbol{\epsilon}^{*\lambda}$, which also enhance ρ_{00}. This effect is seen clearly in the top panel of Fig. 9 for which our qualitative analysis is valid. For ϕ production, where the main contribution comes from the meson-exchange channel (cf. Figs. 2 and 6), ρ_{00} is relatively small, $\rho_{00}<0.05$. But for ω production, where the contribution of the resonance channel is essential, we find $\rho_{00}\sim 0.3$, which is close to an isotropic spin density distribution with $\rho_{00}\simeq\rho_{11}=\rho_{-1-1}\simeq 1/3$.

Figure 10 exhibits the angular distribution of hadronic decays $\phi\to K^+K^-$ and $\omega\to\pi^+\pi^-\pi^0$ in $\pi^- p\to nV$ reactions at $\Delta s^{1/2}=20$ MeV. The top panel corresponds to a calculation of the vector-meson production in the forward direction, $0.9<\cos\theta<1$, where the cross section achieves a maximum, while the bottom panel shows its average value in the full angular interval $-1<\cos\theta<1$. One can see a striking difference between the ϕ and ω cases: an anisotropic distribution for ϕ production ($\mathcal{W}\simeq\frac{3}{2}\sin^2\Theta$) and, within 10% accuracy, a nearly isotropic distribution for ω production ($\mathcal{W}\sim 1$), respectively, which reflect the difference in the corresponding production mechanisms.

A similar difference is predicted for the angular distribution of electrons in $\pi^- p\to nV\to ne^+e^-$ reactions shown in Figs. 11 and 12 at $\Delta s^{1/2}=20$ and 100 MeV, respectively. Again one can see that at $\Delta s^{1/2}=20$ MeV (Fig. 11) the ϕ and ω cases are very different: an anisotropic distribution for ϕ production [$\mathcal{W}\simeq\frac{3}{4}(1+\cos^2\Theta)$] and an isotropic distribution for ω production ($\mathcal{W}\sim 1$), respectively. This pronounced difference disappears at $\Delta s^{1/2}=100$ MeV (Fig. 12).

It should be emphasized that our prediction for the separate decay $\omega\to e^+e^-$ may be tested experimentally, supposing that the corresponding detector acceptance is sufficiently large for distinguishing the sharp ω resonance peak in the dielectron invariant mass distribution sitting on the background of the wide ρ^0 meson contribution. Otherwise one should consider the ω-ρ^0 interference as calculated for unpolarized observables in [17]. However, having in mind that the ρ^0 production is a competing channel to the ω production, where the role of the resonances is expected to be even more important because of the larger number of intermediate

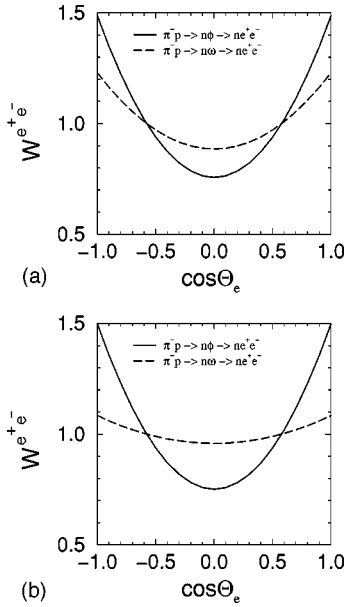

FIG. 11. Electron angular distributions in the reaction $\pi^- p\to nV\to ne^+e^-$ at $\Delta s^{1/2}=20$ MeV. Top panel: the distribution at forward vector-meson production angles; bottom panel: the distribution averaged over the all production angles.

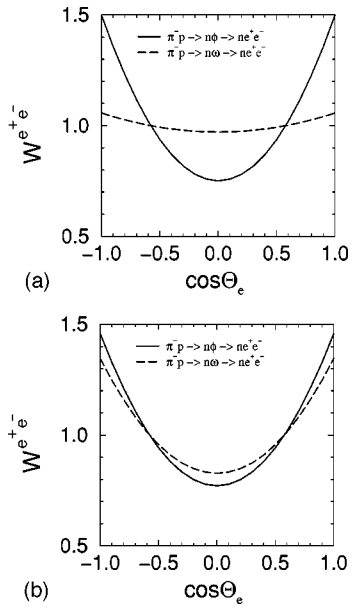

FIG. 12. The same as in Fig. 11 but at $\Delta s^{1/2}=100$ MeV.

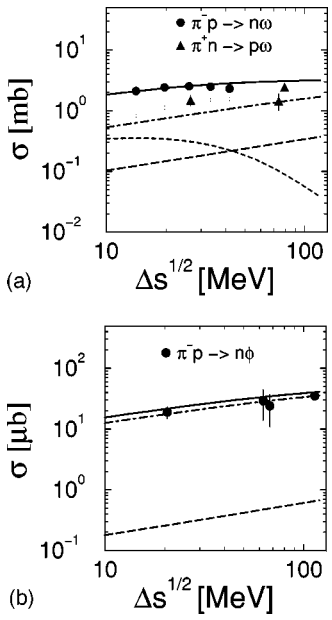

FIG. 13. Total cross sections for the reactions $\pi N \to N\omega$ (top panel) and $\pi^- p \to n\phi$ (bottom panel) as a function of the energy excess $\Delta s^{1/2}$, assuming a constructive interference between meson-exchange and baryonic channels with the parameter set described in the text. Notation as in Fig. 2.

N^* states, we expect that our prediction of an almost isotropic e^+e^- distribution at invariant mass $M_{e^+e^-} \simeq m_\omega$ remains valid, in general, reflecting the role of the baryon resonances in the production mechanism.

Let us now explore the importance of the signs of $g_{\omega\pi\rho}$ and $g_{\phi\pi\rho}$. All above calculations have been performed for positive (negative) values of $g_{\omega\pi\rho}$ $(g_{\phi\pi\rho})$, which lead to a destructive interference between meson-exchange and baryonic channels. The opposite signs of $g_{V\pi\rho}$ cause a constructive interference and change our predictions. First of all, it is impossible to describe the data with otherwise the same set of parameters. In order to achieve a reproduction of the data we have to decrease not only the cutoffs Λ_V^ρ, Λ_B, but also $|g_{\omega\pi\rho}|$ and the resonance couplings $g_{\omega NN*}$. The result of a corresponding calculation is shown in Fig. 13, where we use the lowest value for $|g_{\omega\pi\rho}|$ discussed in Ref. [9], $|g_{\omega\pi\rho}| = 8.3$ GeV^{-1}, and $\Lambda_V^\rho = 1.2$ GeV, $\Lambda_B = 0.6$ GeV and the couplings $g_{\omega NN*}$ are scaled by a factor of 0.44. Since this new parametrization describes the total cross sections equally well as the previous set, we get a similar prediction for the ratio of the averaged amplitudes of ω and ϕ production as shown in Fig. 14, top panel (cf. Fig. 8, bottom panel). So, one cannot distinguish between two parameter sets when considering only unpolarized data. But in the present case of a negative (positive) value of $g_{\omega\pi\rho}$ $(g_{\phi\pi\rho})$, the meson-exchange channels dominate for both reactions and, as a consequence, the prediction of the distribution of ω decay products will be different from the previous case. In Fig. 14 (bottom panel) we show the angular distribution of hadronic decays $\phi \to K^+K^-$ and $\omega \to \pi^+\pi^-\pi^0$ in $\pi^- p \to nV$ reactions at $\Delta s^{1/2}=20$ MeV. Instead of a nearly isotropic distribution for the ω decay shown in Fig. 10, now we get an anisotropic distribution. Therefore, this reaction together with polarization measurements in the ω photoproduction reaction can shed light on the phase of $g_{V\rho\pi}$ and the role of baryon resonance dynamics.

IV. SUMMARY

In summary we have performed a combined analysis of ω and ϕ production in πN reactions near the threshold at the same energy excess. We find that the meson-exchange amplitude alone cannot describe the existing data, even in the

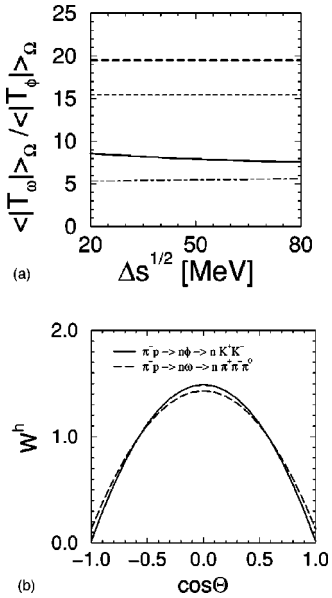

FIG. 14. Top panel: Ratio of the amplitudes of ω and ϕ production averaged over production angle as in top panel of Fig. 8. Notation as in Fig. 2. Bottom panel: Meson angular distributions in the reactions $\pi^- p \to n\phi \to nK^+K^-$ and $\pi^- p \to n\omega \to n\pi^+\pi^-\pi^0$ as in Fig. 10 but for a constructive interference between meson-exchange and baryonic channels.

comparatively narrow energy interval, where our effective model is applicable. Rather, the role of the direct nucleon term and the nucleon-resonance amplitudes is essential. The inclusion of resonance channels gives a natural explanation of the observable ratio of the ω to ϕ production, based on the standard OZI rule conserving partial amplitudes.

The nucleon resonance contributions are very important for the ω production, and therefore we investigate their role in detail. The ωNN^* couplings as well as the phases of the πNN^* couplings are taken from the recent work [16]. It is found that the resonance contributions can influence significantly the total and the differential cross sections at small energy excess as well as the ratio of the averaged amplitudes of ω and ϕ production. For this ratio we get the value 8.7 ± 1.5, which is much smaller than the value based on the standard OZI rule violation. The dominant contributions are found to stem from the nucleon resonances $N_{1/2-}(1535)S_{11}$, $N_{1/2-}(1650)S_{11}$, and $N_{1/2+}(1440)P_{11}$. However, the other resonances become also important with increasing energy excess.

We have shown that the resonance contributions can essentially be tested, on a qualitative level, by measuring the angular distribution of decay particles in the reactions $\pi N \to N\phi \to NK^+K^-$, $\pi N \to N\omega \to N3\pi$, and $\pi N \to NV \to Ne^+e^-$. Near the threshold, for the ϕ production we predict an anisotropic distribution, while for the ω production an isotropic distribution is obtained when assuming $g_{\omega\pi\rho} > 0$. However, in case of an opposite sign we find a stronger meson-exchange channel with an anisotropic ω distribution. Experimentally, these predictions can be tested with the pion beam at the HADES spectrometer at GSI/Darmstadt [46].

It should be stressed that the present investigation is completely based on the conventional meson-nucleon dynamics and, therefore, our predictions may be considered as a necessary background for forthcoming studies of the hidden strangeness degrees of freedom in nonstrange hadrons. Finally, it should be emphasized that our study here is a first step from the point of view of a dynamical treatment of the problem, thus going beyond [9]. The main uncertain part is the poor knowledge of the strong cutoff factors for the virtual nucleon and nucleon resonances which are important for the present consideration. Also, the effects of the final state interaction must be investigated in greater detail, which may be pursued by extending the approach of Refs. [12,35,38,42].

ACKNOWLEDGMENTS

We gratefully acknowledge fruitful discussions with H. W. Barz, R. Dressler, S. B. Gerasimov, L. P. Kaptari, and J. Ritman. One of the authors (A.I.T.) thanks the warm hospitality of the nuclear theory group in the Research Center Rossendorf. This work was supported by BMBF Grant No. 06DR921, the Heisenberg-Landau program, HADES-JINR participation Project No. 03-1-1020-95/2002, and the Russian Foundation for Basic Research under Grant No. 96-15-96426.

APPENDIX A: SPIN-PROJECTION OPERATOR

As mentioned above, our choice of the projection operators $\Lambda_{qq'}(p,M)$, where $q=\alpha$ $(q=\alpha\beta)$ for spin-$\frac{3}{2}$ (-$\frac{5}{2}$) baryons, differs from the commonly used on-shell operators. To clarify this point let us consider the case of spin-$\frac{3}{2}$ particles. The explicit form of the on-shell operator $\overline{\Lambda}_{\alpha\beta}(p,M)$ may be obtained [47] by the boosting of the spinors in the sum

$$\overline{\Lambda}_{\alpha\beta}(p,M) = \sum_r \mathcal{U}^r_\alpha(\mathbf{p}) \otimes \overline{\mathcal{U}}^r_\beta(\mathbf{p}) = -\left[g_{\alpha\beta} - \frac{1}{3}\gamma_\alpha\gamma_\beta - \frac{\gamma_\alpha p_\beta - \gamma_\beta p_\alpha}{3M} - \frac{2p_\alpha p_\beta}{3M^2} \right] \times (\not{p} + M). \tag{A1}$$

Inspection of Eq. (34) shows that, at $p^2=M^2$, the contributions from the second line vanish and consequently $\overline{\Lambda}_{\alpha\beta}(p,M)=\Lambda_{\alpha\beta}(p,M)$. As a result, for example, the calculation of the decay widths in Eqs. (40)–(42) gives the same result by using either Eq. (A1) or Eq. (34).

For $p^2 \neq M^2$, generally speaking, Eq. (A1) is not valid even for the s channel with $\mathbf{p}^2=0$. In this case Eq. (A1) leads to the nonphysical transition for $\alpha=\beta=0$ with $\overline{\Lambda}_{00}(p,M) \sim s-M^2$. To avoid this problem one can use the off-shell generalization of Eq. (A1) with the substitution [18]

$$M \to \sqrt{p^2}. \tag{A2}$$

Now, $\overline{\Lambda}_{00}(p,M)=0$, but $\overline{\Lambda}_{\alpha\beta} \neq \Lambda_{\alpha\beta}$. The main difference between $[\overline{\Lambda}_{\alpha\beta}(p,\sqrt{s})]_{ij}$ and $[\Lambda_{\alpha\beta}(p,M)]_{ij}$ (for the s channel only) arises in this off-shell case because of transitions with $i(j)=3,4$. These transitions are absent in $[\overline{\Lambda}_{\alpha\beta}(p,\sqrt{s})]_{ij}$ but exist in $[\Lambda_{\alpha\beta}(p,M)]_{ij}$ because of the terms in the second line in Eq. (34). The difference is proportional to $\sqrt{s}-M$ and vanishes at $M_{N^*} \to \sqrt{s}$. This is illustrated in Fig. 15, where we show the s channel contributions for $N_{3/2^-}(1700)D_{13}$ and $N_{3/2^+}(1720)P_{13}$ resonances at $\Delta s = 20$ MeV as a function of the ω production angle. For $N_{3/2^+}(1720)P_{13}$ the difference is not seen at all. For $N_{3/2^-}(1700)D_{13}$ this difference is less than 50%; Eq. (A1) results in a symmetric angular distribution, while Eq. (34) leads to slightly asymmetrical one. The same tendency is found for the $N_{3/2^-}(1520)D_{13}$ resonance. It would be interesting to study experimentally this effect. But, unfortunately,

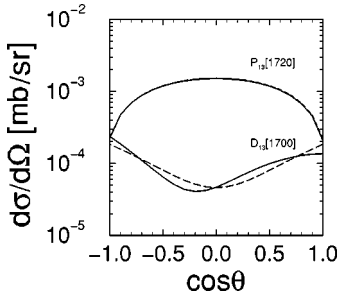

FIG. 15. The s channel contribution for $N_{3/2^-}(1700)D_{13}$ and $N_{3/2^+}(1720)P_{13}$ taken separately for the reaction $\pi^- p \to n\omega$ at $\Delta s = 20$ MeV. Dashed and solid lines correspond to Eqs. (A1) and (A2) and (34), respectively.

in the case of ω production, the dominant contribution comes from spin-$\frac{1}{2}$ resonances with a well defined spin-projection operator. In the energy distribution, which is integrated over the ω production angle, the difference between the two methods becomes very modest.

For the u channel amplitudes with $p^2<0$, the ansatz of Eq. (A2) is not appropriate and one cannot use Eq. (A1). Since the crossing symmetry requires the inclusion of the u channel together with the s channel, one has to employ a universal spin-projection operator, such as $\Lambda=(\not{p}+M)$ for spin-$\frac{1}{2}$ baryons. Note that in our case the dominant contributions come mainly from the s channel amplitudes and the present discussion has a rather methodological character. But nevertheless, taking into account that (i) Eqs. (34) and (35) give a universal prescription for higher spins and coincide on the mass shell with the well-known spin-$\frac{3}{2}$ projector, and (ii) give the correct off-shell behavior for spin-$\frac{1}{2}$ baryons, we choose them in our calculations.

APPENDIX B: ENERGY-DEPENDENT DECAY WIDTH

Following [34] the total resonance decay width is expressed as a sum of weighted partial widths

$$\Gamma(W)=\sum_j \Gamma_j \frac{\rho_j(W)}{\rho_j(M_{N*})}. \tag{B1}$$

Here, Γ_j is the partial width for the resonance decay into the jth channel, evaluated at $W\equiv\sqrt{s}=M_{N*}$. The form of the "phase space" factor $\rho_j(W)$ depends on the decay channel. For a decay of the resonance into two stable particles (e.g., $\pi N,\ \eta N,\ K\Lambda$), it is parametrized by

$$\rho_j(W)=\frac{q_j}{W}B_{l_j}(q_j), \tag{B2}$$

where q_j is the relative momentum of the two particles, l_j denotes their relative orbital momentum, and B_{l_j} stands for the decay probability [48]

$$\begin{aligned} B_0&=1,\\ B_1&=x/\sqrt{1+x^2},\\ B_2&=x^2/\sqrt{9+3x^2+x^4},\\ B_3&=x^3/\sqrt{225+45x^2+6x^4+x^6},\\ B_4&=x^4/\sqrt{11025+1575x^2+135x^4+10x^6+x^8} \end{aligned} \tag{B3}$$

with $x=q_jR$, $R=0.25$ fm. The energy-dependent partial widths have the proper analytic threshold behavior $\propto q_j^{2l_j+1}$ at $q_j\to 0$ and become constant at high energy.

For the quasi-two-body decay, where one of the outgoing particles with mass M_x is unstable and decays further into two stable particles with masses m_2, m_3 (e.g., $\pi\Delta$, $N\rho$, $N\sigma_\epsilon$), the phase space factor reads

$$\rho_j(W)=\int_{m_2+m_3}^{W-m_1}\sigma(M_x)\frac{q_j(M_x)}{W}B_{l_j}(q_j(M_x))dM_x. \tag{B4}$$

The spectral density $\sigma(M_x)$ is chosen in the conventional form

$$\sigma(M_x)=\frac{1}{\pi}\frac{\frac{1}{2}\Gamma_0}{(M_x-m_0)^2+\frac{1}{4}\Gamma_0^2}, \tag{B5}$$

where the parameters M_0 and Γ_0 are given in Table I of [34]. The partial decay widths in Eq. (B1) and the relative orbital momentum l_j in Eq. (B2) are chosen according to Table II of [34].

[1] S. Okubo, Phys. Lett. **5**, 165 (1963); G. Zweig, CERN Report No. 8419/TH 412, 1964 (unpublished); I. Iizuka, Prog. Theor. Phys. Suppl. **37/38**, 21 (1966).

[2] Particle Data Group, C. Caso *et al.*, Eur. Phys. J. C **3**, 1 (1998).

[3] J. Ellis, M. Karliner, D.E. Kharzeev, and M.G. Sapozhnikov, Phys. Lett. B **353**, 319 (1995).

[4] J. Ellis, M. Karliner, D.E. Kharzeev, and M.G. Sapozhnikov, Nucl. Phys. **A673**, 256 (2000).

[5] M.P. Locher and Y. Lu, Z. Phys. A **351**, 83 (1995); D. Buzatu and F.M. Lev, Phys. Lett. B **329**, 143 (1994).

[6] J. Gasser, H. Leutwyler, and M.E. Sainio, Phys. Lett. B **253**, 252 (1991).

[7] D.B. Kaplan and A.V. Manohar, Nucl. Phys. **B310**, 527 (1988); R.D. McKeown, Phys. Lett. B **219**, 140 (1989); E.M. Henley, G. Krein, S.J. Pollock, and A.G. Williams, *ibid.* **269**, 31 (1991).

[8] A.I. Titov, Y. Oh, and S.N. Yang, Phys. Rev. Lett. **79**, 1634 (1997); A.I. Titov, Y. Oh, S.N. Yang, and T. Morii, Phys. Rev. C **58**, 2429 (1998).

[9] A. Sibirtsev and W. Cassing, Eur. Phys. J. A **7**, 407 (2000).

[10] H.J. Lipkin, Phys. Lett. **60B**, 371 (1976).

[11] G. Fäldt and C. Wilkin, Z. Phys. A **357**, 241 (1997); N. Kaiser, Phys. Rev. C **60**, 057001 (1999).

[12] A.I. Titov, B. Kämpfer, and B.L. Reznik, Eur. Phys. J. A **7**, 543 (2000).

[13] B. Friman and H.J. Pirner, Nucl. Phys. **A617**, 496 (1997).

[14] M. Lutz, G. Wolf, and B. Friman, Nucl. Phys. **A661**, 526 (1999).

[15] M. Post and U. Mosel, Nucl. Phys. **A688**, 808 (2001).

[16] D.O. Riska and G.E. Brown, Nucl. Phys. **A679**, 577 (2001).

[17] M. Soyeur, M. Lutz, and B. Friman, nucl-th/0003013.

[18] M. Post, S. Leupold, and U. Mosel, Nucl. Phys. **A689**, 753 (2001).

[19] Y. Oh, A.I. Titov, and T.-S.H. Lee, Phys. Rev. C **63**, 025201 (2001).

[20] M. Benmerrouche, N.C. Mukhopadhyay, and J.F. Zhang, Phys. Rev. D **51**, 3237 (1995), and further remarks and references in [30,31,35,38].

[21] W.S. Chung, G.Q. Li, and C.M. Ko, Phys. Lett. B **401**, 1 (1997).

[22] A.I. Titov, B. Kämpfer, and V.V. Shkyar, Phys. Rev. C **59**, 999 (1999).
[23] K. Nakayama, A. Szczurek, C. Hanhart, J. Haidenbauer, and J. Speth, Phys. Rev. C **57**, 1580 (1998).
[24] K. Nakayama, J.W. Durso, J. Haidenbauer, C. Hanhart, and J. Speth, Phys. Rev. C **60**, 055209 (1999).
[25] DISTO Collabration, F. Balestra *et al.*, Phys. Rev. Lett. **81**, 4572 (1998); Phys. Lett. B **468**, 7 (1999).
[26] E.L. Bratkovskaya, W. Cassing, U. Mosel, O.V. Teryaev, A.I. Titov, and V.D. Toneev, Phys. Lett. B **362**, 17 (1995).
[27] Aachen-Berlin-Hamburg-Heidelberg-München Collaboration, Phys. Rev. **175**, 1669 (1968).
[28] J.D. Bjorken and S.D. Drell, *Relativistic Quantum Mechanics* (McGraw-Hill, New York, 1964).
[29] R. Machleidt, Adv. Nucl. Phys. **19**, 189 (1989).
[30] H. Haberzettl, Phys. Rev. C **56**, 2041 (1997); H. Haberzettl, C. Bennhold, T. Mart, and T. Feuster, *ibid.* **58**, 40 (1998).
[31] R.M. Davidson and R. Workman, Phys. Rev. C **63**, 058201 (2001); **63**, 025210 (2001).
[32] C. Itzykson and J.-B. Zuber, *Quantum Field Theory* (McGraw-Hill, Singapore, 1985).
[33] M. Benmerrouche, N.C. Mukhopadhyay, and J.F. Zhang, Phys. Rev. D **51**, 3237 (1995).
[34] D.M. Manley and E.M. Salesky, Phys. Rev. D **45**, 4002 (1992).
[35] T. Sato and T.-S.H. Lee, Phys. Rev. C **54**, 2660 (1996).
[36] A.I. Titov, T.-S.H. Lee, H. Toki, and O. Streltsova, Phys. Rev. C **60**, 035205 (1999).
[37] Th.A. Rijken, V.G.J. Stoks, and Y. Yamamoto, Phys. Rev. C **59**, 21 (1999).
[38] T. Feuster and U. Mosel, Phys. Rev. C **58**, 457 (1998); **59**, 460 (1999); A. Waluyo, C. Bennhold, H. Haberzettl, G. Penner, U. Mosel, and T. Mart, nucl-th/0008023.
[39] U.-G. Meissner, V. Mull, J. Speth, and J.W. Van Orden, Phys. Lett. B **408**, 381 (1997).
[40] T. Feuster and U. Mosel, Phys. Rev. C **58**, 457 (1998).
[41] O. Krehl, C. Hanhart, S. Krehwald, and J. Speth, Phys. Rev. C **62**, 025207 (2000).
[42] K. Schilling and F. Storim, Nucl. Phys. **B7**, 559 (1968).
[43] A. Baldini *et al.*, *Total Cross Sections of High Energy Particles*, Landolt-Börnstein, New Series, Group I, Vol. 12 (Springer-Verlag, Berlin, 1988).
[44] H. Karami *et al.*, Nucl. Phys. **B154**, 503 (1979).
[45] C. Hanhart and A. Kudryavtsev, Eur. Phys. J. A **6**, 325 (1999); C. Hanhart, A. Sibirtsev, and J. Speth, hep-ph/0107245.
[46] HADES Collaboration, J. Friese *et al.*, GSI Report No. 97-1, 1997 (unpublished); Prog. Part. Nucl. Phys. **42**, 235 (1999).
[47] H. Pilkuhn, *The Interaction of Hadrons* (North-Holland, Amsterdam, 1967).
[48] D.M. Manley, R.A. Arndt, Y. Goradia, and V.L. Teplitz, Phys. Rev. D **30**, 904 (1984).